Fifteen Years of Solution-Processed Photovoltaics

A Research Trajectory in Earth-Abundant Chalcogenide Thin-Film Solar Cells (2010–2026)

Jesús Capistrán-Martínez

Research Trajectory Webinar, October 15, 2026

Centro de Investigaciones en Dispositivos Semiconductores (CIDS)
Instituto de Ciencias, Benemérita Universidad Autónoma de Puebla (BUAP)
ORCID: 0000-0001-8555-5440

Outline

Motivation and Framework

I. Foundations: All-Chemically Deposited Cells (2010)

II. Antimony Sulfide Absorbers (2011–2012)

III. Silver Antimony Sulfide: Structure and Transport (2014–2015)

IV. Band-Gap Engineering by Selenization (2014–2021)

V. Computational Device Design (2021)

VI. Flexible Photovoltaics on Stainless Steel (2024–2025)

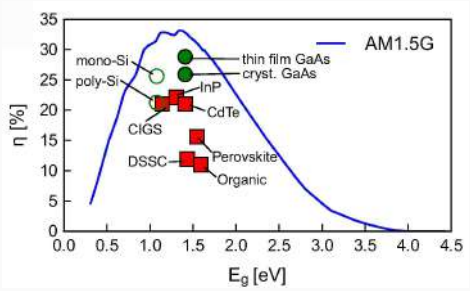
VII. Defect Engineering and Machine Learning (2026)

Synthesis and Outlook

Motivation and Framework

Why Earth-Abundant Thin-Film Photovoltaics?

- Terawatt-scale clean energy requires absorbers that are abundant, non-toxic, and scalable.
- Established technologies rely on scarce or toxic elements: In, Ga, Te (CIGS, CdTe) and Pb (perovskites).
- Working hypothesis since 2010: *metal chalcogenides of Sb, Bi, Sn, Cu and Zn can be deposited from aqueous solutions at low temperature.*
- The **Shockley–Queisser** optimum lies near $E_g \approx 1.3$–1.5 eV for a single junction solar cell under AM1.5 illumination.



Maximum light to electric power conversion efficiency for a solar cell operated at 298.15 K and illuminated with the AM 1.5G

The experimental challenge

Can we *synthesize* a ∼1.5 eV absorber with an all-solution route?

Chemical Bath Deposition: The Enabling Technique

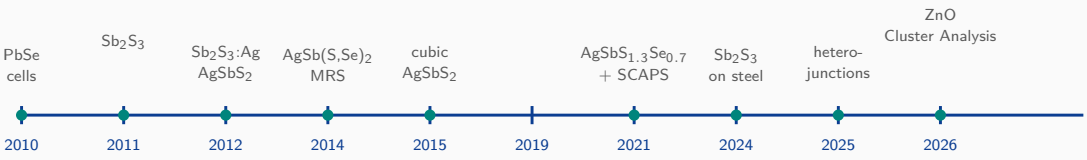
- **Ion-by-ion condensation** from an aqueous bath onto a substrate: no vacuum, no high-temperature equipment.
- Thickness controlled by time and bath chemistry (50–700 nm).
- Chalcogenide source:
  - sulfide: thiourea, thiosulfate;
  - selenide: selenosulfate, selenourea, or Se vapor.
- Compatible with large area and flexible substrates.

Representative condensation reactions

$$2SbCl_3 + 3Na_2S_2O_3 \rightarrow Sb_2(S_2O_3)_3 + 6NaCl,$$
$$Sb_2(S_2O_3)_3 \rightarrow 2Sb^{3+} + 3S_2O_3^{2-},$$
$$Ag_2(S_2O_3) \rightarrow 2Ag^{+} + S_2O_3^{2-},$$
$$S_2O_3^{2-} + H_2O \rightarrow SO_4^{2-} + S^{2-} + 2H^{+},$$
$$Ag^{+} + 2S^{2-} + Sb^{3+} \rightarrow \text{Ag–Sb–S}.$$

The common methodological thread of all eleven works presented here.

Research at a Glance: The Publication Timeline



Two career transitions: UNAM (CIE/IER, Temixco) 2010–2015 $\rightarrow$ BUAP (Puebla) 2019–2026.

Career Stages and Roles

Stage	Years	Institution	Role / output
Research assistant	2010	CIE-UNAM (Dr. P. K. Nair)	Co-author [1]
Master's	2011–2012	CIE/IER-UNAM	1st first-author [3]
PhD	2013–2015	IER-UNAM	$AgSbS_2$ line [4, 5]
Postdoc	2019–2021	IF-BUAP (Dr. M. Pal)	Simulation [6]
	2021	IER-UNAM (collab.)	Solar cells [7]
Postdoc	2024–2026	CIDS-BUAP (Dr. R. Romano-Trujillo)	Steel + ML [8, 10, 11]

CONACYT graduate fellowship (2011–2015); SEP-PRODEP, CONAHCYT and SECIHTI postdoctoral fellowships (2019–2026).

I. Foundations: All-Chemically Deposited Cells (2010)

PbSe Thin Films in All-Chemically Deposited Solar Cells

- Architecture: **TCO/CdS/Sb_2S_3/PbSe**, all layers by sequential CBD [1].
- Two selenide precursors: sodium selenosulfate (SS) and *N,N*-dimethylselenourea (SU).
- **Energy-level engineering:** the CdS/Sb_2S_3 junction alone gives $V_{oc} \leq 595$ mV but almost no current.
- PbSe acts as a p^+ optical absorber: it raises J_{sc} by orders of magnitude.

Champion cell (SU, 150 nm)

V_{oc}=690 mV, J_{sc}=3.5 mA/cm^2, η=0.69 %

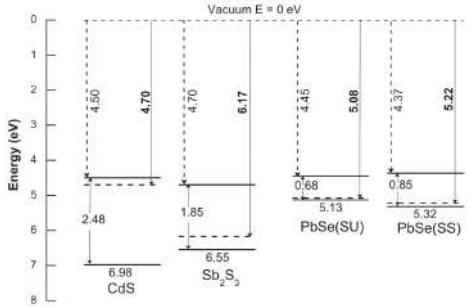


Figure 9. Energy level diagrams of the individual materials constituting the cell structures (values are negative with respect the vacuum level). The numbers in bold are for the Fermi levels.

"PbSe Thin Films in All-Chemically Deposited Solar Cells" [1]

II. Antimony Sulfide Absorbers (2011–2012)

Sb_2S_3: Two Chemical Routes and the J_L Landscape

- Absorber of choice: $\alpha > 10^4$ cm^{-1}, $E_g = 1.7$–1.9 eV [2].
- Two formulations ($SbCl_3$–thiosulfate; antimony tartrate–thioacetamide).
- Crystallization by annealing in N_2 at 250 °C to 300 °C.
- CdS/Sb_2S_3/C-Ag cells reach $V_{oc} \approx 640$ mV, $J_{sc} = 2$–5 mA/cm^2, $\eta = 0.5$–1%.

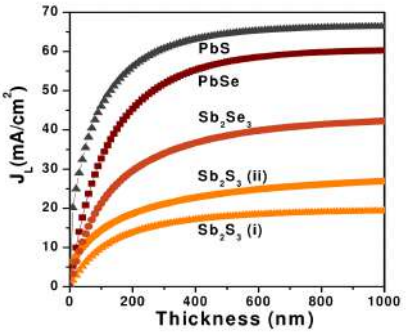


Figure 2. Light generated current density

"Antimony Sulfide Absorbers in Solar Cells" [2]

From Sb_2S_3 to $AgSbS_2$: Silver as a Dopant

- $AgNO_3$ added to the Sb_2S_3 bath; Ag:Sb ratio 0.002–0.4 [3].
- Low Ag content (≤ 0.004): Ag acts as a sensitizer. Then, photoconductivity rises by **3 orders of magnitude**.
- At Ag:Sb $= 0.4$: single-phase cubic **$AgSbS_2$** (cuboargyrite, $a = 0.5652$ nm, $E_g = 1.79$ eV).
- Birth of the silver-antimony-sulfide research line.

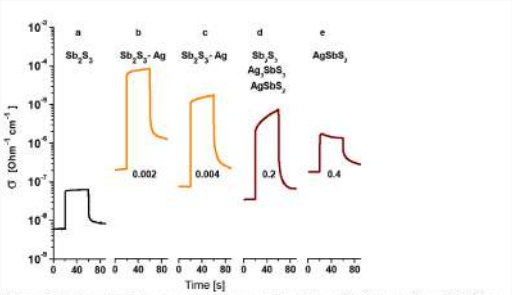


Figure 3. Photoconductivity response of the crystalline films: a, Sb_2S_3; b, Sb_2S_3-Ag (0.002); c, Sb_2S_3-Ag (0.004); d, mixed phase Sb_2S_3/Ag·Sb·S (0.2); e, $AgSbS_2$ (0.4).

"Antimony Sulfide and Silver Antimony Sulfide Absorbers for Thin Film Solar Cells" [3]

Photoconductivity: $Sb_2S_3 : Ag$

$$\sigma_{\text{ph}} : \underbrace{\sim 10^{-8}}_{Sb_2S_3} \rightarrow \underbrace{7.4 \times 10^{-5}}_{\text{Ag-doped}} \ \Omega^{-1}\,\text{cm}^{-1}$$

III. Silver Antimony Sulfide: Structure and Transport (2014–2015)

Amorphous-to-Cubic Transformation of $AgSbS_2$

- As-deposited Ag–Sb–S films ($Ag/(Ag+Sb) = 0.31$) are **amorphous** [5].
- Heating at 150 °C to 320 °C gives **cubic $AgSbS_2$ (cuboargyrite)**, PDF 17-0456.
- Crystallinity: 3.7% (150 °C) → 98% (280 °C).
- Crystal size (Scherrer analysis of the XRD peaks) reaches only 8 nm to 11 nm.
- E_g : 2.03 eV (amorphous) → 1.79 eV (cubic).

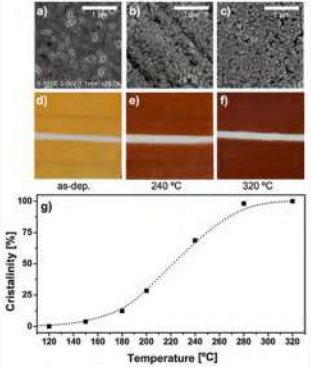


Figure 3 Scanning electron micrographs (scale bar 1 μm) of (a) as-deposited film and after heating at (b) 240 and (c) 320 °C (d–f) appearance of the films placed on a ruled white paper with an etched middle patch of 2 mm width used for step-thickness measurement; (g) "crystallinity" of the films defined as the ratio (%) of integrated area of (111) and (200) peaks in Fig. 2 of a film to that of the film heated at 320 °C (dotted line serves as a visual aid)

"Photoconductive Thin Films of $AgSbS_2$ with Cubic Crystalline Structure in Solar Cells" [5]

XRD Evidence: Cubic $AgSbS_2$ from Annealing

- Grazing-incidence XRD (1°) tracks the **amorphous** → **crystalline** conversion of the Ag–Sb–S film.
- Increasing the annealing temperature progressively sharpens the peaks of **cubic $AgSbS_2$ (cuboargyrite, PDF 17-0456)**.
- At 200 °C to 320 °C the pattern matches a single-phase cubic structure (log-scale panel c).
- Above 350 °C the material decomposes — the processing window is narrow.

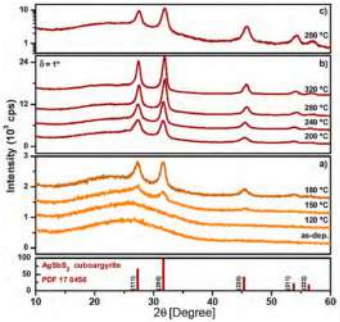


Figure 2 (a) XRD patterns recorded at gracing incidence 1° for as-deposited film of 150 nm in thickness and then heated at 120, 150, and 180 °C with the crystalline peaks matching those of the mineral cuboargyrite (PDF 17-0456) shown in the bottom panel for the cubic structure of $AgSbS_2$; (b) progressively improving crystalline component illustrated by increasing crystalline peak areas as the film is heated from 200 to 320 °C; (c) XRD intensity plotted in log-scale to establish that the crystalline material formed is of single phase cubic-$AgSbS_2$.

"Photoconductive Thin Films of $AgSbS_2$ with Cubic Crystalline Structure in Solar Cells" [5]

Photoconductivity, Mobility and the J_{L} Ceiling

- Under $1000\,\mathrm{W/m^2}$: $\sigma_d = 8.4 \times 10^{-7}$, $\sigma_p = 1.6 \times 10^{-5}\ \Omega^{-1}\,\mathrm{cm}^{-1}$ ($\times 20$ photosensitivity).
- Light-generated current from the absorption coefficient and the AM1.5G spectrum:

$$J_{\mathrm{L}}(d) = \sum (0.1q) N_{\mathrm{ph}}(h\nu)\left[1 - e^{-\alpha d}\right] \Delta(h\nu)$$

- Even at $\sim 1\,\mu\mathrm{m}$, $J_{\mathrm{L}} \leq 16\,\mathrm{mA/cm^2}$.

Best $AgSbS_2$ cell

SnO_2:F/CdS/$AgSbS_2$(420 nm)/C-Ag

V_{oc}	0.615 V
J_{sc}	$1.67\,\mathrm{mA/cm^2}$
FF	0.54
η	0.57 %

Conclusion

A supplementary absorber or gap reduction is required $\rightarrow$ selenization.

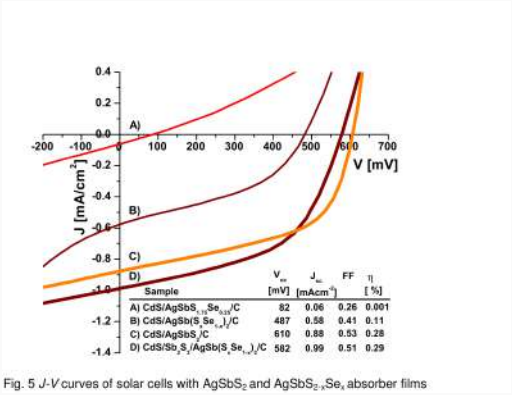
IV. Band-Gap Engineering by Selenization (2014–2021)

$AgSb(S,Se)_2$: The First Solid Solutions (2014)

- S→Se substitution lowers E_g and raises the carrier mobility ($AgSbSe_2$: $\mu \approx 1500\,\mathrm{cm}^2/\mathrm{V\,s}$).
- Amorphous $AgSbS_2$ crystallizes to cubic $AgSbS_2$ in N_2; heating in **Se vapor** yields **$AgSb(S,Se)_2$** [4].
- Composition from Vegard's law:

$$a_{\mathrm{ss}} = x\, a_{\mathrm{Se}} + (1 - x)\, a_{\mathrm{S}}$$

- Two-absorber cell improves the current: $Sb_2S_3/AgSb(S,Se)_2 \rightarrow \eta = 0.29\,\%$.



Sample	V_{oc} [mV]	J_{sc} [mAcm^{-2}]	FF	η [%]
A) CdS/$AgSbS_{1.5}Se_{0.5}$/C	82	0.06	0.26	0.001
B) CdS/$AgSb(S_xSe_{1-x})_2$/C	487	0.58	0.41	0.11
C) CdS/$AgSbS_2$/C	610	0.88	0.53	0.28
D) CdS/Sb_2S_3/$AgSb(S_xSe_{1-x})_2$/C	582	0.99	0.51	0.29

Fig. 5 *J-V* curves of solar cells with $AgSbS_2$ and $AgSbS_{2-x}Se_x$ absorber films

"Silver Antimony Sulfide-Selenide for Thin Film Solar Cells" [4]

$AgSbS_{1.3}Se_{0.7}$: Toward the Ideal Gap (2021)

- Three-step route: CBD **$AgSbS_2$** (700 nm) in contact with a CBD **amorphous-Se** film (300 nm), heated at 180 °C in argon [7].
- fcc (cuboargyrite) structure preserved; composition $AgSbS_{1.3}Se_{0.7}$ from Vegard's law.
- E_g : 1.80 → 1.47 eV; σ_{ph} an order of magnitude higher.

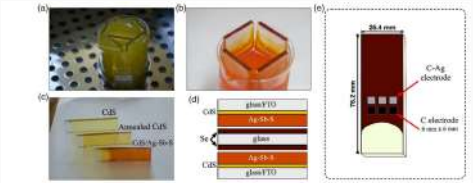


Figure 1. a) Chemical deposition of CdS thin film (80 nm) at 80 °C in 55 min on FTO; b) chemical deposition of Ag – Sb – S (350 nm) on FTO/CdS for 3 h 30 min and repeated for a second time to obtain a film of 700 nm in cumulative thickness; and c) appearance of these films, FTO/CdS, annealing in air at 350 °C for 15 min, and after the Ag – Sb – S deposition. d) Arrangement for heating at 180 °C for selenization of FTO/CdS/Ag – Sb – S/Se/glass/Se films, also prepared by chemical deposition. e) Solar cells of FTO/CdS/$AgSbS_xSe_y$ /colloidal graphite paint heated at 280 °C with silver paint electrodes.

"Silver Antimony Sulfide Selenide Thin-Film Solar Cells via Chemical Deposition" [7]

Cell performance

SnO_2:F/CdS/$AgSbS_{1.3}Se_{0.7}$(700 nm)/C-Ag

V_{oc}	0.527 V
J_{sc}	2.07 mA/cm^2
FF	0.60
η	0.65 %

Roadmap

$\eta \approx 10.8\,\%$ if $J_{sc} \to J_L = 29\,\text{mA/cm}^2$.

V. Computational Device Design (2021)

Cu_3BiS_3: Combining Experiment with SCAPS-1D

- **Cu_3BiS_3 (CBS, wittichenite)**: Cd-free, earth-abundant, defect-tolerant (lone-pair $6s^2$ on Bi^{3+}) [6].
- Films by thermal diffusion of CBD **Bi_2S_3/CuS** stacks at 300 °C to 350 °C: $E_g = 1.55$–1.75 eV, p-type, μ_p up to $88\,cm^2/V\,s$.
- Those experimental parameters are loaded into SCAPS-1D to simulate a single heterojunction.
- Comparing a CdS buffer with a Cd-free Bi_2S_3 buffer: $\eta = 6.8\% \rightarrow 7.6\%$.

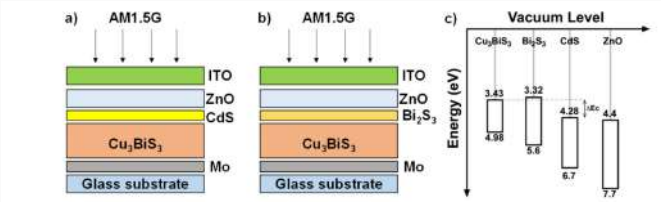


Fig. 6. Schematic of CBS solar cell structure in substrate configuration: (a) typical configuration with a CdS buffer layer, (b) the proposed design with a suitable Bi_2S and (c) flat band energy diagram of the proposed cell.

"Theoretical Evaluation of Emerging Cd-free Cu_3BiS_3 Based Solar Cells Using Experimental Data of Chemically Deposited Cu_3BiS_3 Thin Films" [6]

Why a Cd-Free Buffer Wins: Band Alignment

- **CBS/CdS**: cliff-type offset, $\Delta E_c = -0.85$ eV $\Rightarrow$ strong interface recombination and V_{oc} collapse.
- **CBS/Bi_2S_3**: spike-type offset, $\Delta E_c = +0.11$ eV $\Rightarrow$ reduced recombination and higher V_{oc}.
- Both CBS and Bi_2S_3 are orthorhombic $\Rightarrow$ better lattice matching.
- Ohmic Mo/CBS back contact ($+0.03$ eV hole barrier).

Built-in voltage

$$qV_{\mathrm{bi}} = \Delta E_c + E_{g(p)} - E_{g(n)} + k_B T \ln \frac{p_p n_n}{n_{i(p)} n_{i(n)}}$$

Design rule

A small *spike* (0 to $+0.4$ eV) is optimal; *cliffs* ($\Delta E_c < 0$) must be avoided.

SCAPS-1D Device Design: Energy Band Diagrams

- The experimentally measured Cu_3BiS_3 parameters were loaded into SCAPS-1D: absorber 1 µm, buffer 50 nm, ZnO (50 nm)/ITO (100 nm) front contact.
- Simulated output: η increases from 6.8 % (CdS) to 7.6 % (Bi_2S_3); V_{oc} from 0.400 to 0.508 V.

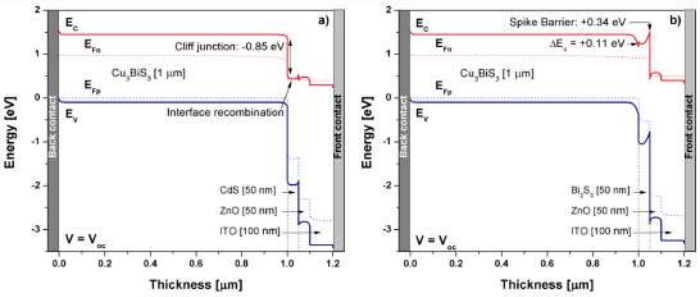


Fig. 8. Energy band diagrams corresponding to (a) CBS/CdS solar cells and (b) CBS/Bi_2S_3 solar cell.

"Theoretical Evaluation of Emerging Cd-free Cu_3BiS_3 Based Solar Cells Using Experimental Data of Chemically Deposited Cu_3BiS_3 Thin Films" [6]

VI. Flexible Photovoltaics on Stainless Steel (2024–2025)

Sb_2S_3 on Stainless Steel: Crystallization in Air

- First CBD of Sb_2S_3 on **stainless-steel** (SS430/SS304) [9].
- Sequential deposition at 2 °C; crystallization at 300 °C for 5 min in ambient air.
- Orthorhombic stibnite, (020) preferred orientation; E_g : 2.36 → 1.71–1.78 eV.
- Sequential layers heal cracks and pinholes ⇒ flexible, substrate-configuration cells.

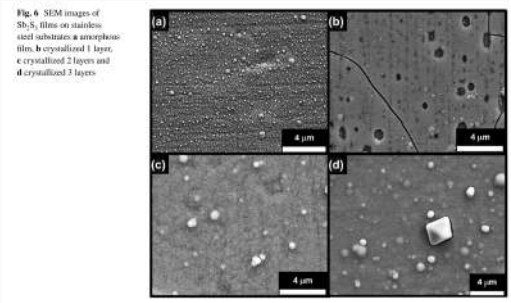


Fig. 6 SEM images of Sb_2S_3 films on stainless steel substrates **a** amorphous film, **b** crystallized 1 layer, **c** crystallized 2 layers and **d** crystallized 3 layers

"Crystallization of Antimony Sulfide Films on Stainless Steel Substrates Obtained by Sequential Chemical Bath Deposition" [9]

$AgSb(S,Se)_2$ on SS304: Band-Gap Modulation in Air

- CBD $AgSbS_2$ on SS304 + one-step selenization in ambient air [8].
- Solid solutions $AgSbS_{1.7}Se_{0.3}$ and $AgSbS_{1.5}Se_{0.5}$ (Vegard's law); Se up to 11.4 at %.
- E_g tuned from 1.71 to 1.47 eV — ideal for PV.
- Ohmic C/SS304/$AgSb(S,Se)_2$/C contact ⇒ flexible solar cells.

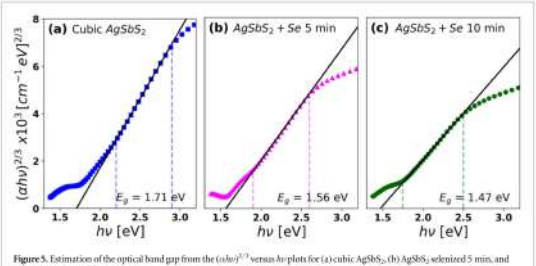


Figure 5. Estimation of the optical band gap from the $(\alpha h\nu)^{2/3}$ versus $h\nu$-plots for (a) cubic $AgSbS_2$, (b) $AgSbS_2$ selenized 5 min, and (c) $AgSbS_2$ selenized for 10 min.

"Silver Antimony Sulfide Thin Films and Its Selenization on Stainless Steel Substrates by Chemical Bath Deposition" [8]

$AgSb(S,Se)_2$/CdS Heterojunctions on SS304

- Selenization time tuned 15–60 min (Se vapor 400 °C, substrate 175 °C); optimal 30 min: 13 at % Se, $E_g = 1.58$ eV, $\sigma = 8.84 \times 10^{-7}\ \Omega^{-1}\,\mathrm{cm}^{-1}$ [10].
- Dark I–V: $I_s \sim 10^{-7}$ A, $V_{th} = 0.72$–0.80 V, $n = 3.0$–4.4.

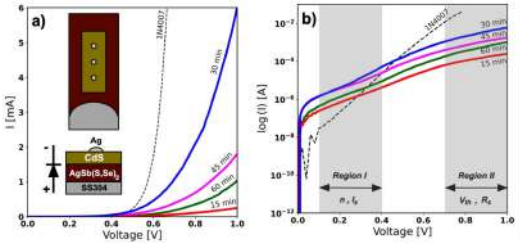


Fig. 8. Dark I-V characterization of $AgSb(S,Se)_2$ heterojunctions: a) Linear dark I-V plot shows the rectification region for V < 0.4 V and threshold region for V > 0.7 V. b) Semi-logarithmic plot of the dark I-V focus on Region I to analyze the diode ideality factor (n) and saturation current (I_s) while Region II wa$_s$ used to extract V_{th} and R_s.

VII. Defect Engineering and Machine Learning (2026)

Oxygen-Rich ZnO by Microwave CBD

- New material and method: **MWCBD** of ZnO under varied $Zn(NO_3)_2$ concentration and pH [11].
- Hexagonal wurtzite; tunable rod morphologies (flat, pencil, globular, hollow tips).
- Oxygen-rich stoichiometry (Zn/O ≈ 0.68–0.80), $E_g = 3.17$–3.25 eV.
- Dominant yellow-orange deep-level emission at 579 nm to 595 nm $\Rightarrow$ oxygen-related defects.

The analytical challenge

PL emission bands overlap, and defect assignments depend strongly on growth conditions.

Solution

Combine **PL deconvolution** with **unsupervised machine learning (DBSCAN)** to extract objective, recurring emission groups.

PL Deconvolution + DBSCAN: Seven Defect Clusters

- PL spectra deconvoluted (Gaussian model, $R^2 = 0.999$); DBSCAN ($\varepsilon = 0.08$, min_samples $= 2$) clusters the emission energies of all nine films into seven groups.

Cluster assignments

#	Energy (eV)	Defect
1	1.74	O_{Zn} (red)
2	2.10	O_i (yellow)
3	2.35	V_{Zn} (green)
4	2.81	O_i/V_{Zn}/complex
5	3.01	Zn_i (violet)
6	3.17	H-related
7	3.27	NBE

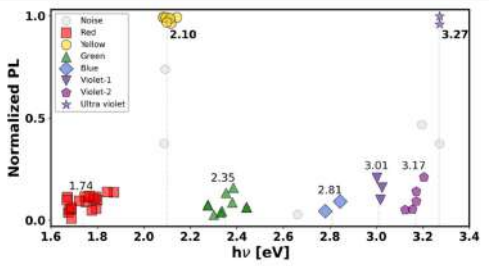


Fig. 6. Identification of native point defects in oxygen-rich ZnO films by clustering analysis of photoluminescence emission energies. Distinct clusters were identified using the DBSCAN algorithm implemented via Scikit-learn Python library.

"Defect Identification in Oxygen-Rich ZnO Thin Films Synthesized by Microwave Chemical Bath Deposition via Photoluminescence Deconvolution and DBSCAN Clustering" [11]

Synthesis and Outlook

The Six Research Lines — A Coherent Map

	Materials	Period	Contribution
A	$CdS/Sb_2S_3/PbSe$, PbS	2010–2011	All-CBD cells, $\eta \leq 1\%$, large area
B	Sb_2S_3, Sb_2S_3:Ag	2011–2012	Ag sensitization, $\times 10^3$ photoconductivity
C	$AgSbS_2$, $AgSb(S,Se)_2$	2012–2021	E_g: 1.9→1.47 eV; best thin-film cell
D	$Cu_3BiS_3 + Bi_2S_3$	2021	SCAPS-1D: Cd-free design, $\eta = 7.6\%$
E	Sb_2S_3, $AgSb(S,Se)_2$ on steel	2024–2025	First CBD on steel; air selenization
F	ZnO (MWCBD)	2026	PL deconvolution + DBSCAN defect mapping

One material family, one method

Chalcogenides + chemical bath deposition =

earth-abundant, scalable, vacuum-free photovoltaics.

Key Achievements in Numbers

Experimental milestones

- **11** peer-reviewed works, 2010–2026.
- Best $AgSbS_2$ cell: $\eta = 0.57\%$, $V_{oc} = 0.615$ V [5].
- Best $AgSbS_{1.3}Se_{0.7}$ cell: $\eta = 0.65\%$, FF $= 0.60$ [7].

Design and analysis milestones

- Band-gap engineering of Sb_2S_3, $AgSbS_2$ and selenized $AgSbS_2$ films: **1.47–2.03 eV**.
- Cu_3BiS_3/Bi_2S_3 simulated at **7.6%** [6].
- First CBD on stainless steel + air selenization [8].
- Oxygen-rich ZnO: 7 defect clusters by DBSCAN [11].

Conclusions

- A single methodological thread: chemical bath deposition has supported fifteen years of research across five institutions and three career stages.
- **Materials:** from PbSe and Sb_2S_3, through the $AgSbS_2/AgSb(S,Se)_2$ family, to Cu_3BiS_3 and ZnO.
- **Band-gap engineering** by S→Se substitution brought the absorber from 2.03 to 1.47 eV, very close to the Shockley–Queisser optimum.
- **Substrates:** glass/TCO → stainless steel, opening the route to flexible, substrate-configuration devices.
- **Methodology:** increasingly quantitative — device simulation (SCAPS-1D) and machine learning (DBSCAN) now complement synthesis and characterization.

Outlook: Where the Research Goes Next

Materials and devices

- Recrystallization of Sb_2S_3 and $AgSbS_2$ solar absorbers (e.g. $SbCl_3$ flux) to enlarge grains and close the J_{sc}–J_L gap.
- Mo buffer layers to relieve thermal-expansion mismatch on steel.
- Double-absorber stacks and p^+ back-surface fields.

Data-driven materials science

- Expand PL + clustering to other solution-processed oxides and chalcogenides.
- Couple defect databases with device simulation.
- Use AI agents to accelerate data analysis.
- Target: earth-abundant, Cd-free, flexible solar cells.

Thank you — questions welcome.

Acknowledgments

CIE/IER-UNAM (Temixco)

- Dr. P. Karunakaran Nair
- Dr. M. T. Santhamma Nair
- Dr. Ralph A. Zingaro (Texas A&M)

Instituto de Física, BUAP

- Dr. Mou Pal

CIDS-BUAP

- Dr. R. Romano-Trujillo
- Dr. R. Galeazzi, Dr. J. M. Gracia-Jiménez
- Dr. A. Coyopol, Dr. N. R. Silva-González
- Dr. E. Rosendo, Dr. C. Morales, Dr. G. García

Funding
CONACYT, SEP-PRODEP, CONAHCYT, SECIHTI, VIEP-BUAP, PAPIIT-UNAM.

References

1. P. K. Nair, E. Barrios-Salgado, J. Capistrán, M. L. Ramón, M. T. S. Nair, and R. A. Zingaro. **"PbSe Thin Films in All-Chemically Deposited Solar Cells".** In: *Journal of The Electrochemical Society* 157.10 (2010), pp. D528–D537. DOI: 10.1149/1.3467844.
2. P. K. Nair, R. González Lua, M. Calixto Rodríguez, J. Capistrán Martínez, O. GomezDaza, and M. T. S. Nair. **"Antimony Sulfide Absorbers in Solar Cells".** In: *ECS Transactions* 41.4 (2011), pp. 149–156. DOI: 10.1149/1.3628620.
3. J. Capistrán M., M. T. S. Nair, and P. K. Nair. **"Antimony Sulfide and Silver Antimony Sulfide Absorbers for Thin Film Solar Cells".** In: *MRS Online Proceedings Library*. Vol. 1447. 2012. DOI: 10.1557/opl.2012.1085.
4. J. Capistrán-Martínez, M. T. S. Nair, and P. K. Nair. **"Silver Antimony Sulfide-Selenide for Thin Film Solar Cells".** In: *MRS Online Proceedings Library*. Vol. 1675. 2014. DOI: 10.1557/opl.2014.859.

References

5 J. Capistrán-Martínez and P. K. Nair. **"Photoconductive Thin Films of $AgSbS_2$ with Cubic Crystalline Structure in Solar Cells".** In: *physica status solidi (a)* 212.12 (2015), pp. 2869–2876. DOI: 10.1002/pssa.201532496.

6 J. Capistrán-Martínez, D. Loeza-Díaz, D. Mora-Herrera, F. Pérez-Rodríguez, and M. Pal. **"Theoretical Evaluation of Emerging Cd-free Cu_3BiS_3 Based Solar Cells Using Experimental Data of Chemically Deposited Cu_3BiS_3 Thin Films".** In: *Journal of Alloys and Compounds* 867 (2021), p. 159156. DOI: 10.1016/j.jallcom.2021.159156.

7 J. Capistrán-Martínez, M. T. S. Nair, and P. K. Nair. **"Silver Antimony Sulfide Selenide Thin-Film Solar Cells via Chemical Deposition".** In: *physica status solidi (a)* 218.11 (2021), p. 2100058. DOI: 10.1002/pssa.202100058.

References

[8] J. Capistrán-Martínez, R. Romano-Trujillo, J. M. Gracia-Jiménez, A. Coyopol, N. R. Silva-González, G. García, R. Galeazzi, F. G. Nieto-Caballero, E. Rosendo, and C. Morales. **"Silver Antimony Sulfide Thin Films and Its Selenization on Stainless Steel Substrates by Chemical Bath Deposition".** In: *Physica Scripta* 99.12 (2024), p. 125963. DOI: 10.1088/1402-4896/ad911b.

[9] I. G. Márquez, R. Romano-Trujillo, J. M. Gracia-Jiménez, R. Galeazzi, A. Coyopol, N. R. Silva-González, J. Capistrán-Martínez, G. García, F. G. Nieto-Caballero, and C. Morales. **"Crystallization of Antimony Sulfide Films on Stainless Steel Substrates Obtained by Sequential Chemical Bath Deposition".** In: *Journal of Materials Science: Materials in Electronics* 35 (2024), p. 2087. DOI: 10.1007/s10854-024-13834-4.

References

[10] J. Capistrán-Martínez, R. Romano-Trujillo, J. M. Gracia-Jiménez, A. Coyopol, N. R. Silva-González, G. García, R. Galeazzi, F. G. Nieto-Caballero, E. Rosendo, and C. Morales. **"Heterojunctions of Silver Antimony Sulfide Selenide Fabricated on Stainless Steel Substrates Using CBD and Selenization in Ambient Air".** In: *Journal of Alloys and Compounds* 1012 (2025), p. 178345. DOI: 10.1016/j.jallcom.2024.178345.

[11] J. Capistrán-Martínez, R. Galeazzi, R. Romano-Trujillo, J. M. Gracia-Jiménez, N. R. Silva-González, A. Coyopol, E. Rosendo, C. Morales, and G. García. **"Defect Identification in Oxygen-Rich ZnO Thin Films Synthesized by Microwave Chemical Bath Deposition via Photoluminescence Deconvolution and DBSCAN Clustering".** In: *Ceramics International* 52 (2026), pp. 36541–36550. DOI: 10.1016/j.ceramint.2026.06.155.